Journal of Applied Polymer Science

A highly selective electrochemical sensor for nifedipine based on layer-by-layer assembly films from polyaniline and multiwalled carbon nanotube

Qiguan Wang,[1] Rongna Zhao,[1] Sumin Wang,[1] Hao Guo,[1] Jinhua Li,[1] Hongwei Zhou,[1] Xinhai Wang,[2] Xinming Wu,[1] Yan Wang,[1] Weixing Chen,[1] Wenzhi Zhang[1]

[1]Scientific Research Innovation Team of Solidification Theory and Functional Materials, Shaanxi Key Laboratory of Photoelectric Functional Materials and Devices, School of Materials and Chemical Engineering, Xi'an Technological University, Xi'an, 710021, People's Republic of China

[2]School of Chemistry and Chemical Engineering, Henan University, Kaifeng, 475004, People's Republic of China

Correspondence to: S. M. Wang (E-mail: suminwang@163.com) and X. H. Wang (E-mail: xinhaiwanghenu@163.com)

ABSTRACT: An uniformly distributed film consisting of polyaniline (PANI) nanoparticles and carboxylic acid functionalized multiwalled carbon nanotubes (MWNTs-COOH) was successfully assembled on ITO plates from a layer-by-layer (LBL) method by using electrostatic interactions as the main driving force. The good conjugation between PANI nanoparticles and MWNTs-COOH resulted in significant electrochemical performance variation of the obtained films. In addition, the assembled MWNT-COOH/PANI/ITO showed synergistic effect to the electrochemical oxidation of nifedipine (NIF) when used as a sensor. Compared with bare ITO, the oxidation potential of NIF can be decreased about 170 mV on MWNT-COOH/PANI/ITO, and the lower detection limit of NIF was as low as 1.0×10^{-6} mol/L. In addition, the assembled electrode gave no responses to interferences such as glucose, urea, ascorbic acid, and trisodium citrate, which showed high selectivity for recognition and quantification of NIF. © 2016 Wiley Periodicals, Inc. J. Appl. Polym. Sci. **2016**, *133*, 43452.

KEYWORDS: actuators; conducting polymers; self-assembly; sensors

Received 31 July 2015; accepted 17 January 2016
DOI: 10.1002/app.43452

INTRODUCTION

Carbon nanotubes (CNTs) possessing high conductance, tensile strength, chemical stability, capable of promoting the electron-transfer reactions of important biomolecules such as cytochrome *c*, dopamine, ascorbic acid, exhibited promising application in electrochemical sensors, and biosensors.[1–4] Polyaniline (PANI), one of the most popular and promising conducting polymers, behaving controllable conductivity, environmental stability, interesting redox properties, and exceptional electrocatalytic activity, has been widely used in preparation of biosensors and sensor arrays which possess excellent interference-free performance for the assay of glucose, urea, and triglycerides.[5–9] Significant research efforts have been made to fabricate nanostructured PANI/CNT composites because they could provide synergistic results, enhancing the thermal and mechanical stability, processability, electrical conductivity, and electrocatalytic activity of the materials,[10–14] by using various approaches from *in situ* electropolymerization to interfacial polymerization with template-directed or template-free approaches.[15–18] Besides, layer-by-layer (LBL) self-assembly methodology is a versatile, straightforward method for the fabrication of nanostructured films with controlled compositions, which has become an effective way to prepare CNT/PANI films.[19–22]

The LBL assembly strategy was herein used to prepare thin films composed of PANI and carboxylic acid functionalized multiwalled carbon nanotube (MWNT-COOH). Due to the protonation of imine (—N═) and amine (—NH—) groups, PANI can have net positive charges.[23,24] Meanwhile, MWNT-COOH can be negatively charged by ionization of the carboxylic acid groups which yielded carboxylate anions (COO^-) in aqueous solution.[21,25] Thus, behaving like weak polyelectrolytes, PANI and MWNT-COOH can be readily used for the LBL process. Moreover, the LBL process can also be driven by the hydrogen bonding interaction between the amine groups of PANI and the carboxylic acid groups of MWNTs-COOH (Figure 1).[26,27] Therefore, under such multiple interactions, alternatively dipping indium-tin-oxide (ITO) or quartz slides in PANI and

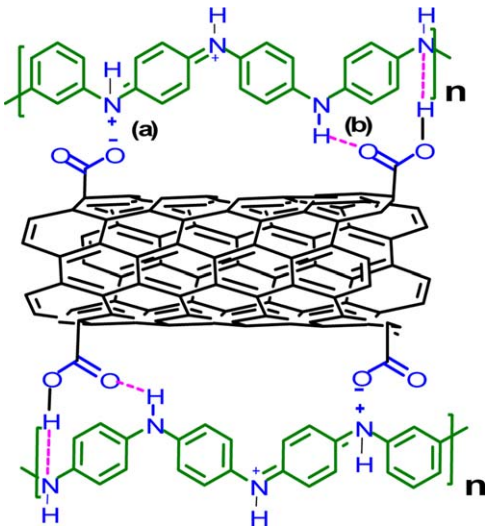

Figure 1. Schematic view of LBL film assembled based on multiple interactions [electrostatic (a), hydrogen bonding (b)] between the positively charged PANI and the negatively charged MWNTs-COOH. [Color figure can be viewed in the online issue, which is available at wileyonlinelibrary.com.]

MWNT-COOH dispersions can lead to a stable and uniform MWNT-COOH/PANI film, showing strong conjugation between PANI and MWNT-COOH. Unfortunately, few documents have been reported on the application of such films especially in photoelectric and electrochemical areas.

As a calcium channel blocker, nifedipine (NIF) has been widely used in the treatment of angina pectoris, arterial hypertension and various cardiovascular diseases. However, its overdose is toxic in nature and may cause severe dizziness, pounding heartbeats, nausea, vomiting, etc. Therefore, from health concern, a low cost, sensitive, and easy monitor of NIF is of great importance. Voltammetry has gained importance in chemical analysis due to its low-cost operation, enhanced sensitivity, and accuracy of measurement. Relative to the extensively studied electroreduction of NIF,[28–30] the determination of NIF by electrooxidation is more convenient because of no need to remove oxygen from the system. However, up to now only few documents have been reported on the determination of NIF based on electro-oxidation by Sentürk *et al.*[31] and Srivastava *et al.*[32] by using an activated glassy carbon electrode and α-cyclodextrins/MWNT paste electrode respectively. Compared with the glassy carbon, MWNT based electrodes will be expected to show more active catalytic behaviors toward NIF because of its superior electric properties, which might be enhanced further by incorporation of some electroactive substances such as the conducting polymer PANI.

Here we will report that the assembled MWNT-COOH/PANI LBL films on ITO exhibited an excellent catalytic effect on the electrochemical oxidation of NIF with good stability and selectivity, mainly due to the synergistic effect of MWNT-COOH and PANI originated from the conjugation and charge transfer between them, which will find potential applications as biosensors.

EXPERIMENTAL

Materials

All reagents and chemicals were used as received unless otherwise noted. MWNTs-COOH (—COOH % = 2.56 wt %, purity >95%, external diameter 20–30 nm, length 10–30 μm) were obtained from Chengdu Institute of Organic Chemistry, Chinese Academy of Science. PANI in its emeraldine base form, was prepared chemically by direct oxidation of aniline using the method developed by MacDiarmid *et al.*[33] NIF was purchased from Sigma. Stock solution of NIF (1×10^{-3} mol/L) was prepared by dissolving an appropriate amount of NIF in methanol (HPLC grade). Britton–Robinson (BR) buffer was prepared by mixing the acid mixture containing phosphoric acid (0.04 mol/L), acetic acid (0.04 mol/L), and boric acid (0.04 mol/L). Buffer solutions were adjusted by adding the necessary amount of NaOH solution (0.20 mol/L) to obtain the appropriate pH value. Milli-Q water (18 MΩ/cm), analytical reagents of *N,N*-dimethylformamide (DMF) and *N,N*-dimethylacetamide (DMAc) were used.

Preparation of Dispersions for LBL Self-Assembly Process

The concentration and the pH value of PANI and MWNTs-COOH dispersions used in the self-assembly process were taken from literature.[21,23,25] A total of 100 mg of emeraldine base of PANI was first dissolved in 5 mL of DMAc by stirring overnight and then was sonicated for 12 h. The solution was then filtered to remove traces of undissolved PANI particles. Then the above prepared solution was diluted by 50 mL of H_2O, and was adjusted to pH = 3 by 1*M* HCl before filtered through a membrane with the pore size $\phi = 0.22$ μm. Under those conditions, a stable aqueous dispersion of PANI could be obtained. MWNT-COOH dispersions were made by ultrasonicating 5 mg of MWNTs-COOH in 10 mL of Milli-Q water for 10 h, and then the pH value of the solution was adjusted to 3 with 1*M* HCl.

Preparation of LBL Assembly Films

MWNT-COOH/PANI LBL films were fabricated manually using PANI and MWNT-COOH aqueous dispersions. Typically, a cleaned quartz or ITO slide previously ultrasonicated in a piranha solution (mixture of 98% H_2SO_4 and 30% H_2O_2, v/v 70:30) for 30 min was first dipped in the PANI dispersion for 1 h, followed by rinsing with water and drying with nitrogen flow at room temperature. The substrate was then dipped in the MWNT-COOH dispersion for 1 h, rinsed, and dried. This leads to the deposition of one bilayer of MWNT-COOH/PANI on both sides of the substrate. The desired numbers of bilayers can be obtained by repetition of above steps.

Preparation of Reference Electrodes

The reference electrodes of PANI/ITO were prepared by dipping a cleaned quartz or ITO slide previously treated by a piranha solution in the PANI dispersion for 1 h, followed by rinsing with water and drying with nitrogen flow at room temperature. The MWNT-COOH/ITO reference electrode was prepared by deposition of two drops of MWNT-COOH solution on bare ITO and then dried at 50 °C in vacuum for 24 h.

Characterization

UV–vis spectra were obtained by a Shimadzu 1901 UV–vis spectrophotometer. Scanning electron microscope (SEM) images were collected by a Quant 400 instrument. The real-time

spectroscopic ellipsometer (Ellipso Technology, Elli-SE-F) with a Xe arc lamp (350 − 820 nm) was applied to measure the thickness of the multilayer film. By using the cleaned reference substrate as reference, more than three to five sampling points were measured to obtain the average thickness. The surface chemistry of LBL film was analyzed by using a PHI 5400 X-ray photoelectron spectrometer (XPS). All spectra were calibrated with the C1s photoemission peak for sp^2 hybridized carbons at 284.5 eV. Curve fitting of the photoemission spectra was done after a Shirley type background subtraction. Infrared absorption spectra (FTIR-RAS) of sample surfaces were collected by the reflection–absorption method using a JASCO FT/IR-4100 spectrometer equipped with a reflector and an MCT-Mid detector, using a bare ITO plate as the reference surface. Cyclic voltammetry (CV) were carried out on a CHI 660C electrochemical workstation with the electroactive films assembled on ITO plates as the working electrode, a saturated calomel electrode (SCE) as the reference electrode and a Pt wire as the counter electrode. The working electrode area was 0.25 cm^2, which was always kept immersed in the electrolyte solution during the data collection.

RESULTS AND DISCUSSION

Film Fabrication and Characterization

Multilayer films were obtained by alternatively dipping hydroxyl group functionalized slide into the PANI dispersion and MWNT-COOH dispersion. In the case the pH value for PANI solution was 2.5–4.5, PANI can be protonated by protonic acid such as HCl, which yields a positively charged PANI suspension.[21,23] Simultaneously, carboxylic acid groups on the surface of MWNTs-COOH possess enough negative charges to maintain stable dispersion when the pH value of the solution is over than 2.[21,25] In this study, it is mainly resulted from the presence of electrostatic interactions between PANI polycation and MWNT-COOH polyanion that makes the LBL deposition available. Furthermore, hydrogen bonding interactions between the amine groups of PANI and carboxylic acid groups of MWNTs-COOH was also existed,[26,27] which may assist the electrostatic interactions to drive the formation of the LBL films.

The assembly process of the LBL multilayer films was monitored by UV–vis spectroscopy for each deposition cycle with PANI as the starting layer followed by MWNT-COOH layer. Figure 2 showed the UV–vis absorption spectra of MWNT-COOH/PANI multilayer films with various bilayer numbers, in which two obvious absorption bands attributed to π–π^* transition of benzoid rings at 320 nm and n–π^* transition of quinoid rings in PANI near 650 nm were found.[34,35] Meanwhile, a faint band attributed to polarons–π^* electronic transition were observed at 450 nm, which showed the presence of cation radicals that produced by the protonation of N atoms in PANI. Furthermore, it is observed that the absorption value at 328 and 640 nm was linearly increased with the increase of bilayer numbers (inset in Figure 2). This indicates a stepwise and regular growth in thickness for the MWNTs-COOH/PANI LBL films. By means of the optical ellipsometry, the thickness of the MWNT-COOH/PANI multilayer film was characterized using a cleaned quartz slide as reference, yielding thickness of around

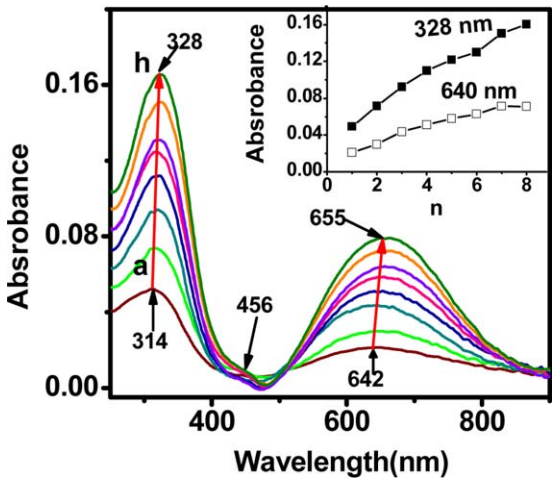

Figure 2. UV–vis absorption spectra of MWNT-COOH/PANI/quartz with increasing numbers of bilayers (a: 1-bilayer, b: 8-bilayer). Inset: absorbance at 328 and 640 nm with the increased numbers of bilayers. [Color figure can be viewed in the online issue, which is available at wileyonlinelibrary.com.]

25 nm for 1-bilayer film and around 200 nm for 8-bilayer film, which also showed the regular deposition of MWNT-COOH/PANI bilayers on the quartz slide.

Moreover, the absorption bands of π–π^* transition and n–π^* transition of PANI on the assembled film were red shifted gradually with increasing the numbers of assembled bilayers, as shown from the arrows in Figure 2. In detail, the absorption bands at 314 and 642 nm for the 1-bilayer LBL film [Figure 2(a)] were red shifted to 328 and 655 nm for the 8-bilayer MWNT-COOH/PANI LBL film [Figure 2(h)]. This showed the presence of strong conjugation between PANI and MWNT-COOH in the assembled film, whose strength can be enhanced gradually with the increase of assembled bilayer numbers.

The conjugation between PANI and MWNT-COOH in the assembled films can also be reflected from CV data. The CVs of MWNT-COOH/PANI/ITO [Figure 3(A)], PANI/ITO [Figure 3(B(a))] and MWNT-COOH/ITO [Figure 3(B(b))] were recorded in 30:70 (v/v) methanol/BR buffer solution at pH = 2 in the range of −0.2 to 1.2 V at the scan rate of 50 mV/s. PANI/ITO [Figure 3(B(a))], shows a reversible redox behavior with an anodic peak at 0.048 V. The CV curve of MWNTs-COOH [Figure 3(B(b))] is quasi-rectangular along the x-axis without any redox peaks. After assembled by one layer of MWNT-COOH, the redox behavior of PANI/ITO was significantly changed. The oxidation peak of PANI at 0.048V [Figure 3(B(a))] was positively shifted to 0.367 V for 1-bilayer MWNT-COOH/PANI/ITO [Figure 3(A(a))], due to the charge transfer from PANI to MWNT-COOH. Furthermore, as the number of the bilayers of MWNT-COOH/PANI on ITO plates was increased from 1 to 15, the oxidation potential of PANI was linearly positively shifted from 0.367 to 0.569 V [Figure 3(A,C)], which indicated the continuous enhancement of charge transfer in the conjugation system of PANI and MWNT-COOH. In addition, the oxidation current values were also linearly increased with the increase of bilayer numbers [Figure 3(D)],

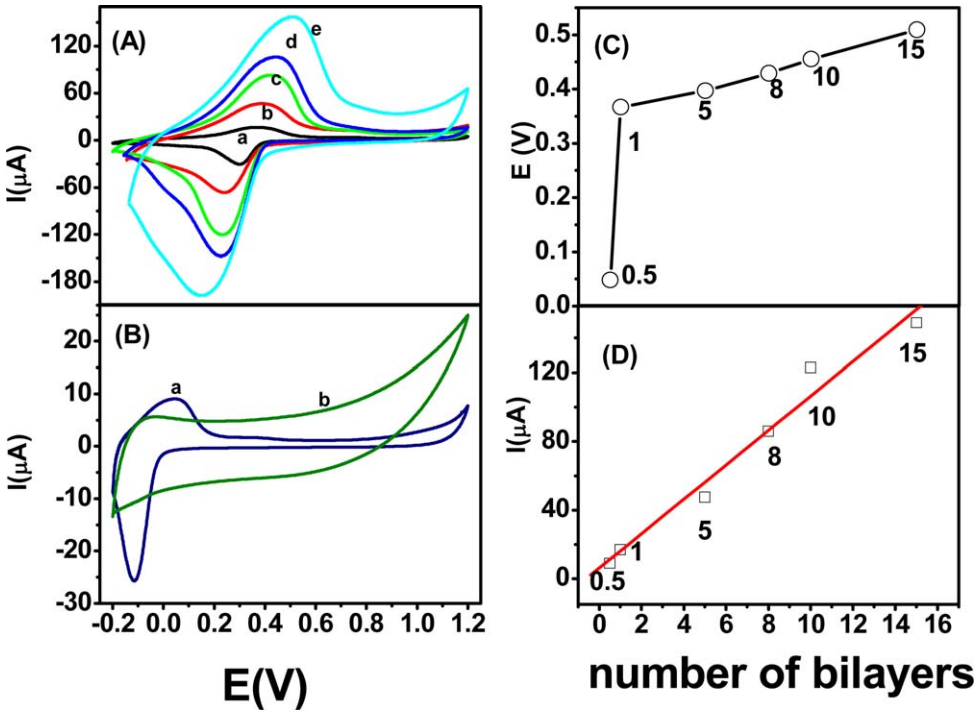

Figure 3. (A) CVs of MWNT-COOH/PANI/ITO films with 1-bilayer (a), 5-bilayer (b), 8-bilayer (c), 10-bilayer (d), and 15-bilayer (e), respectively; (B) cyclic voltammogram of PANI/ITO (a) and MWNT-COOH/ITO (b); (C) The relation of oxidation potential with the numbers of bilayers; (D) The relation of peak current with the numbers of bilayers. The bilayer number for the reference PANI/ITO was denoted as 0.5. Supporting electrolyte: 30:70 (v/v) methanol/BR buffer solution at pH = 2, scan rate: 50 mV/s. [Color figure can be viewed in the online issue, which is available at wileyonlinelibrary.com.]

which verified the homogeneous growth of PANI by such an assembly process.

Scanning electron microscopy was monitored to characterize the surface morphologies of the MWNT-COOH/PANI/ITO, as shown in Figure 4. From the SEM image of PANI/ITO [Figure 4(a)], the large, granular crystalline domains[36] of PANI particles were significantly clustered on the substrate, with the size range 500–1000 nm. However, for the SEM images of an 8-bilayer MWNT-COOH/PANI/ITO film as shown from Figure 4(b), the size of PANI domains was considerably decreased on the slide. On the contrary, a uniformly distributed film was formed consisting of debundled MWNTs [see the arrows in inset of Figure 4(b)] surrounded by highly dispersed PANI nanoparticles, which shows the densely packing and the interconnected networks. In the LBL process, the PANI and MWNT-COOH can be served as the growth template for each other, which controlled the position, size, and morphology of the components directed by the electrostatic and hydrogen bonding interactions.

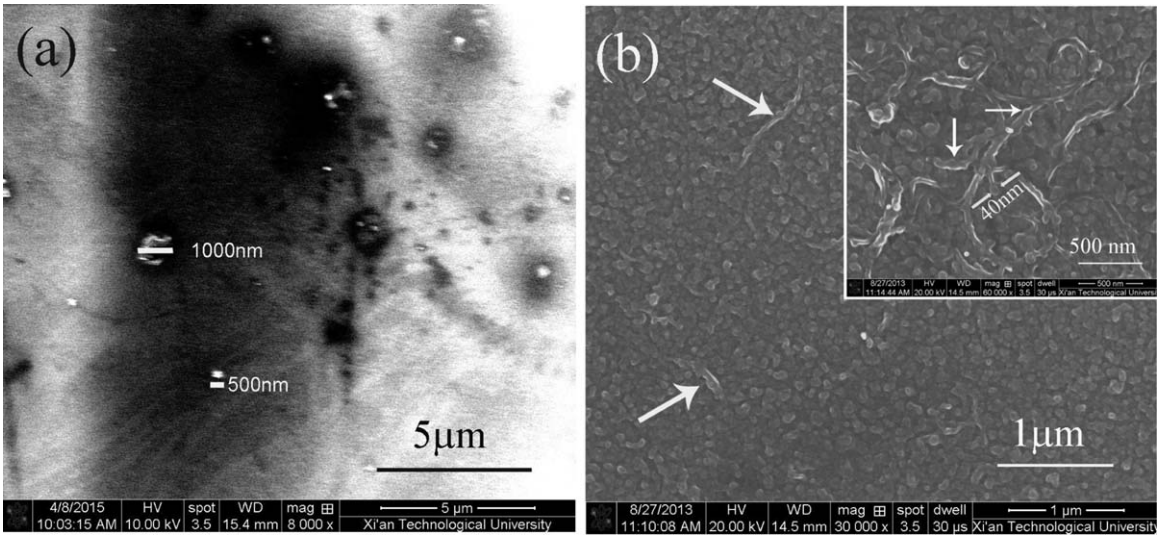

Figure 4. SEM images of the surface of PANI/ITO (a), 8-bilayer MWNT-COOH/PANI/ITO (b) and the magnified image (inset in b).

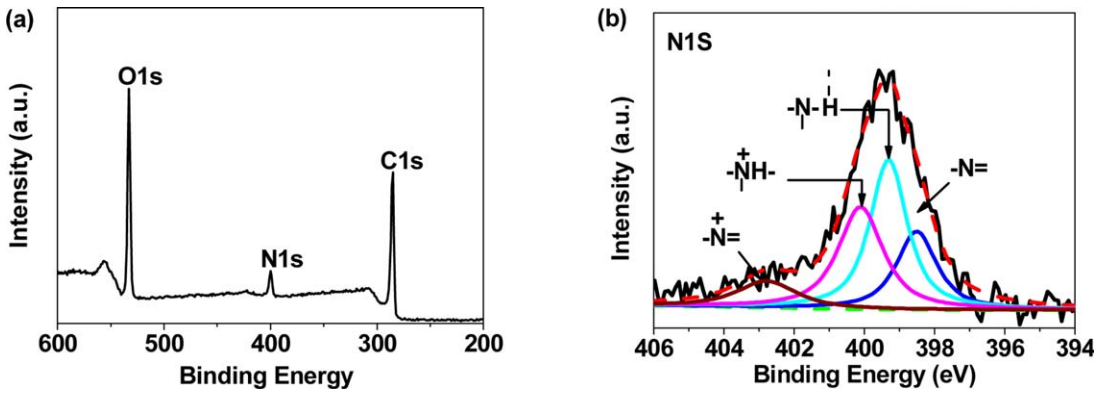

Figure 5. XPS spectra of an 8-bilayer MWNT-COOH/PANI/ITO film. Survey scan (a) and N 1s spectra (b). [Color figure can be viewed in the online issue, which is available at wileyonlinelibrary.com.]

Thus, uniformly distributed PANI nanoaparticles and single MWNTs were formed on the slide. The magnified image [inset in Figure 4(b)] clearly revealed that in the film the size of PANI nanoparticles was in the nanometer scale (40–50 nm), which closely adhere to the wall of MWNTs-COOH [see the arrows in Figure 4(b)].

The presence of electrostatic and hydrogen bonding interactions within the MWNT-COOH/PANI LBL films can be seen from XPS analysis. Figure 5 shows the XPS spectra of an 8-bilayer of MWNT-COOH/PANI/ITO film. The survey scan spectrum [Figure 5(a)] shows that the films consist of a considerable amount of oxygen, nitrogen and carbon elements. The typical N1s spectra of the assembled film [Figure 5(b)] were deconvoluted into four component peaks, centered at 398.5, 399.3, 400.1, and 402.7 eV, respectively. The peak centered at 398.5 eV is assigned to the N1s feature of imide (═N─) in PANI. However, the N1s peak of ─NH─ at 399.3 eV showed a lower binding energy shift compared with the reported value 399.7 eV.[37,38] This is because of the formation of hydrogen bonding in which ─NH─ acts as hydrogen donor, making the nitrogen atoms more electronegative due to the electron transfer from hydrogen acceptor.[39] Additionally, the two peaks with higher binding energy at 400.1 and 402.7 eV could be attributed to $\text{─HN}^{+}\text{─}$ and $\text{═N}^{+}\text{─}$ in PANI units, respectively, indicating the presence of electrostatic interactions in the assembled films.

The presence of hydrogen bonding interactions between PANI and MWNT-COOH in the assembled film was further illustrated by FTIR-RAS spectra. Figure 6 shows the FTIR-RAS spectra of MWNT-COOH/ITO [Figure 6(a)], 8-bilayer MWNT-COOH/PANI/ITO [Figure 6(b)] and PANI/ITO [Figure 6(c)], which all exhibits similar absorption bands associated with the C═C or C═N stretching in PANI or MWNT-COOH at 1450–1610 cm^{-1}.[40] The region of the C═O in carboxylic acid group ranging from 1700 to 1750 cm^{-1} was focused as it can reflect the bonding state of carboxylic acid. As shown in Figure 6(a), for MWNT-COOH/ITO, the absorption bands at 1743 and 1687 cm^{-1} were assigned to the C═O stretching of the carboxylic acid groups, in free monomer and hydrogen bonded dimer state, respectively.[41] However, for the MWNT-COOH/PANI/ITO film [Figure 6(b)], the absorption intensity of peak at 1741 cm^{-1} representing the free monomer state was decreased and that of peak at 1697 cm^{-1} associated with the hydrogen bonded state was increased, because of the hydrogen bonding between MWNT-COOH and PANI.

Encouragingly, the assembled LBL films showed good stability. For the 8-bilayer films of MWNT-COOH/PANI/ITO soaked in acidic aqueous solution at pH = 2 for 15 min, it was found that the CVs showed almost the same as that before soaking. Furthermore, the CVs of assembled films were also unchanged after stayed in air for 6 months. In addition, the 8-bilayer MWNT-COOH/PANI/ITO showed the satisfactory stability toward the mild ultrasonication of 70 W for 1 min in H_2O. The good stability of the multilayer film upon storage, soaking and ultrasonication is very useful for potential applications in biosensors.

Electrocatalytic Effects on Nifedipine

Figure 7 shows the response of the modified electrode toward NIF, the important calcium channel blocker, with the

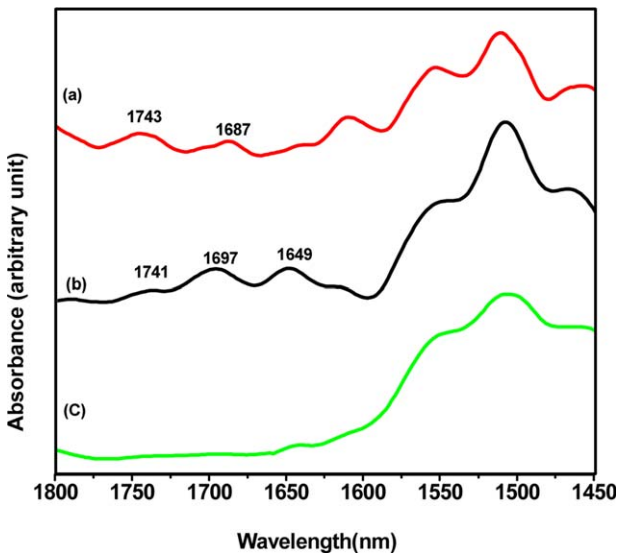

Figure 6. FTIR-RAS spectra of MWNT-COOH/ITO (a), 8-bilayer MWNT-COOH/PANI/ITO film (b), and PANI/ITO (c). [Color figure can be viewed in the online issue, which is available at wileyonlinelibrary.com.]

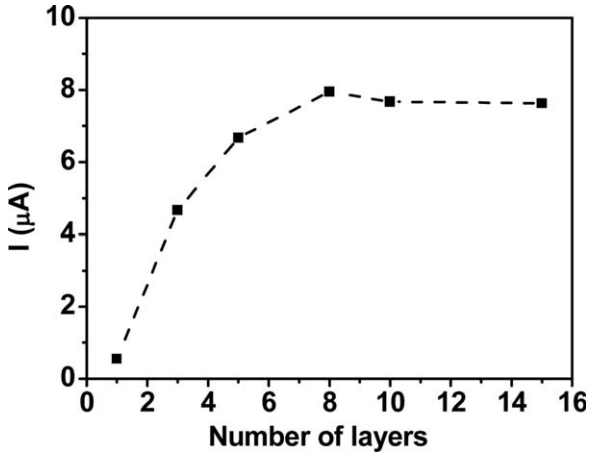

Figure 7. Relationship of the number of bilayers of MWNT-COOH/PANI/ITO with the peak current of NIF (4.0×10^{-5}mol/L) in the 30:70 (v/v) methanol/BR buffer solution at pH = 2.

concentration of 4×10^{-5} mol/L. As seen from Figure 7, the oxidation current of NIF at 0.95 V was increased with the increase of the number of MWNT-COOH/PANI bilayers, due to the progressively loading of MWNTs-COOH and PANI nanoparticles. When the assembled bilayer number reached 8, the oxidation current showed no increase any more.

Figure 8(A) shows the CVs of the 8-bilayer MWNT/PANI/ITO (a), bare ITO (b), PANI/ITO (c), and MWNT-COOH/ITO (d) electrodes toward NIF (4×10^{-5} mol/L) in 30:70 (v/v) methanol/BR buffer solution at pH = 2 in the range of +0.6 to +1.2 V. For the bare ITO, an irreversible oxidation peak of NIF was found at 1.12 V [Figure 8(A(b))]. However, in the case of PANI/ITO [Figure 8(A(c))], the oxidation peak of NIF cannot be found because of the strong electrostatic repulsion between the protonated PANI and the protonated NIF which inhibits approaching of NIF to the electrode surface, thus retarding the oxidation of NIF on the electrode. In the case of the MWNT-COOH/ITO electrode [Figure 8(A(d))], because the MWNTs-COOH have excellent electronic transport properties as well as the strong adsorptive ability to NIF which is induced by the electrostatic and hydrogen bonding interactions between them [Figure 8(B)], the oxidation potential of NIF was shifted negatively to 1.03 V. Regrettably, the background current of NIF on MWNT-COOH/ITO is so strong that the oxidation peak of NIF at 1.03 V is too weak to be observed [Figure 8(A(d))].

As a sharp contrast, in the case of the assembled 8-bilayer MWNT-COOH/PANI/ITO electrodes used, the oxidation peak of NIF became much more significant and was largely negatively shifted to 0.95V [Figure 8(A(a))]. This electrochemical performance enhancement can be attributed to the synergistic oxidation toward NIF from both MWNT-COOH and PANI. On the one hand, NIF could be easily absorbed by the MWNT-COOH/PANI/ITO compared with MWNT-COOH/ITO because the presence of charge transfer from PANI to MWNT-COOH makes the electron density of MWNT-COOH increased, which leads to improved electrostatic and hydrogen bonding interactions between MWNT-COOH and NIF [Figure 8(B)]. On the other hand, the electrons come from the oxidation of NIF could be easily transferred to PANI because of the electron-accepting of

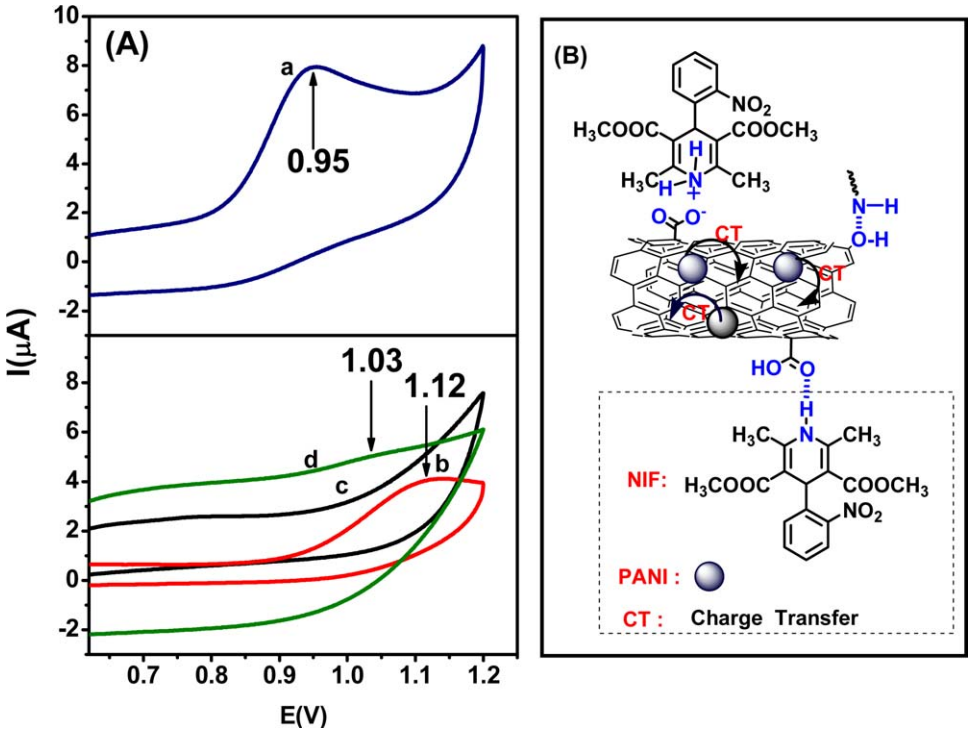

Figure 8. (A) CVs of the 8-bilayer MWNT-COOH/PANI/ITO (a), bare ITO (b), PANI/ITO (c), and MWNT-COOH/ITO (d) toward NIF solution (4.0×10^{-5}mol/L) in 30:70 (v/v) methanol/BR buffer solution at pH = 2. Scan rate: 50 mV/s. (**B**) Schematic representation of adsorption of NIF on the surface of MWNTs-COOH. [Color figure can be viewed in the online issue, which is available at wileyonlinelibrary.com.]

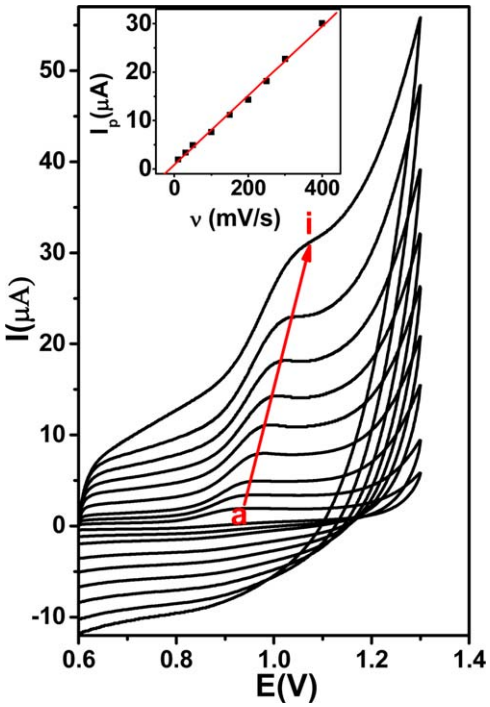

Figure 9. CVs of NIF (2.0×10^{-5} mol/L) in 30:70 (v/v) methanol/BR buffer solution at pH = 2 on an 8-bilayer MWNT-COOH/PANI/ITO electrode at different scan rate (mV/s): (**a**) 10, (**b**) 30, (**c**) 50, (**d**) 100, (**e**) 150, (**f**) 200, (**g**) 250, (**h**) 300, and (**i**) 400 . Inset: The linear relationship of peak current (I_p) of NIT to scan rate (ν). [Color figure can be viewed in the online issue, which is available at wileyonlinelibrary.com.]

protonated PANI, which was conjugated with the MWNT-COOH. Both aspects lead to the facile oxidation of NIF on MWNT-COOH/PANI/ITO. Compared with the bare ITO, the oxidation potential of NIF on the 8-bilayer MWNT-COOH/PANI/ITO multilayer films was shifted negatively up to 170 mV (from +1.12 to +0.95 V vs. SCE). It is more significant than the β-cyclodextrin (β-CD) and MWNT paste electrode which

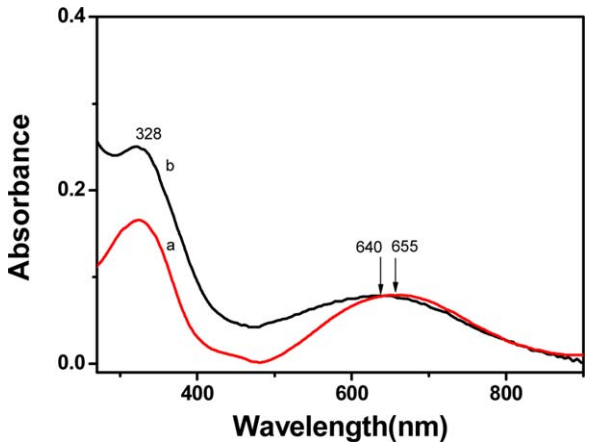

Figure 10. UV–vis absorption spectra of an 8-bilayer MWNT-COOH/PANI/quartz (**a**) and that after treated by the NIF (4.0×10^{-3} mol/L) in 30:70 (v/v) methanol/BR buffer solution (pH = 2) for 30 min (**b**). [Color figure can be viewed in the online issue, which is available at wileyonlinelibrary.com.]

can make the oxidation potential of NIF decreased 60 mV than the bare electrode.[32] Moreover, due to the presence of more electrochemical active compounds on the 8-bilayer MWNT-COOH/PANI/ITO, the oxidation current was increased double times that of bare ITO.

Figure 9 shows the CVs of NIF (2×10^{-5} mol/L) solution on the 8-layer MWNT-COOH/PANI/ITO electrode at different scan rates. From Figure 9, it can be seen that the electrochemical oxidation of NIF is irreversible in nature. Moreover, with the increase of scan rates, the oxidation potential of NIF at the surface of the 8-bilayer MWNT-COOH/PANI/ITO was positively shifted, along with the increase of the peak current. In addition, the peak current of NIF showed a proportional relation to the scan rate in the range 10–400 mV/s (inset of Figure 9), which reveals the oxidation of NIF on the MWNT-COOH/PANI/ITO should be an adsorption controlled process. This is mainly resulted from the electrostatic and hydrogen bonding interactions between MWNT-COOH/PANI/ITO and NIF [Figure 8(B)].

The charge transfer interactions between NIF and PANI on the assembled film were further clarified by comparing the UV–vis spectrum of the 8-bilayer MWNT-COOH/PANI/quartz [Figure 10(a)] with that [Figure 10(b)] after dipped in the NIF solution of methanol/BR buffer (pH = 2) for 30 min. As shown in Figure 10, when the 8-bilayer MWNT-COOH/PANI/quartz was treated with NIF solution (4.0×10^{-3} mol/L), the absorbance intensity at 328 nm was significantly increased because of the deposition of NIF on the assembled film under electrostatic and hydrogen bonding interactions. Moreover, the absorption band at 655 nm attributed to n–π^* transition of quinoid rings in PANI [Figure 10(a)] was blue shifted to 640 nm [Figure 10(b)] due to the charge transfer from NIF to PANI.

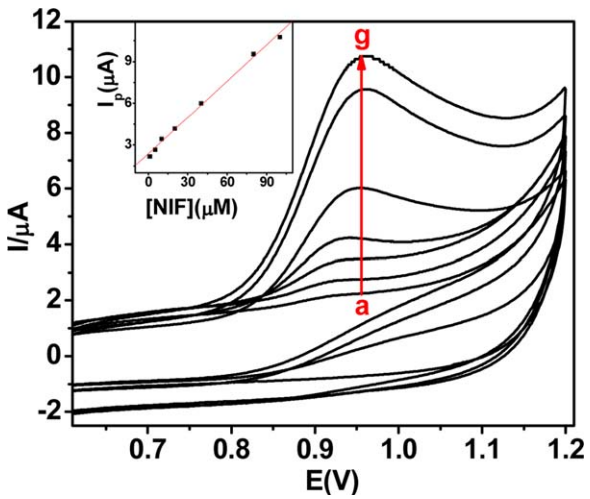

Figure 11. CVs of NIF with different concentrations (mol/L): (**a**) 1.0×10^{-6}, (b) 5.0×10^{-6}, (**c**) 1.0×10^{-5}, (**d**) 2.0×10^{-5}, (**e**) 4.0×10^{-5}, (**f**) 8.0×10^{-5}, and (**g**) 1.0×10^{-4} in 30:70 (v/v) methanol/BR buffer solution at pH = 2 on an 8-bilayer of MWNT-COOH/PANI/ITO electrode at scan rate of 50 mV/s. Inset: the linear relationship of peak current (I_p) to the concentration of NIF. [Color figure can be viewed in the online issue, which is available at wileyonlinelibrary.com.]

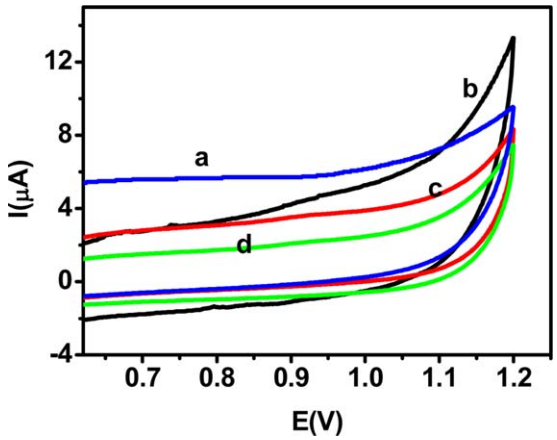

Figure 12. CVs of glucose (**a**), urea (**b**), ascorbic acid (**c**), and trisodium citrate (**d**) solutions with the concentration of 1.0×10^{-4} mol/L on an 8-bilayer MWNT-COOH/PANI/ITO electrode in 30:70 (v/v) methanol/BR buffer solution at pH = 2. Scan rate: 50 mV/s. [Color figure can be viewed in the online issue, which is available at wileyonlinelibrary.com.]

The CVs response of the 8-bilayer MWNT–COOH/PANI/ITO in 30:70 (v/v) methanol/BR buffer solution at pH = 2 containing different concentrations of NIF was shown in Figure 11. The calibration curve in inset of Figure 11 shows that the peak current was increased linearly as NIF concentrations were increased from 1.0×10^{-6} to 1.0×10^{-4} mol/L at the scan rate 50 mV/s. It follows the equation as I_p (A) = 0.0869 C_{NIF} (M) + 2.378 (R = 0.99476), where I_p is the redox peak current, C is the concentration of NIF. Compared with that (8.0×10^{-5} mol/L) measured by the activated glassy carbon electrode,[31] the lower limit (1.0×10^{-6} mol/L) for NIF concentration in the linearity ranges of calibration plots was decreased measured upon the MWNT-COOH/PANI/ITO electrode.

In order to evaluate the selectivity of the MWNT-COOH/PANI/ITO electrode for the electrochemical determination of NIF, the commonly used interferences for the determination of NIF were investigated at the surface of the 8-bilayer MWNT-COOH/PANI/ITO. The assembled electrode showed no response for the interferences such as glucose, urea, ascorbic acid, and trisodium citrate solutions with the concentration level of 1×10^{-4} M (Figure 12). This suggests that the determination of NIF cannot be affected by common interfering species that are often present along with NIF. Therefore, MWNT-COOH/PANI/ITO can be considered as a good electrochemical sensor for recognition and quantification of NIF.

CONCLUSIONS

Electrostatic and hydrogen bonding interactions can drive the LBL process to construct a uniform distributed film consisting of PANI nanopariticles and debundling MWNTs-COOH, forming a good conjugation system. Synergistic effect of PANI and MWNT-COOH to the electrochemical oxidation of NIF benefiting from the composite components was observed for the assembled film when used as a sensor. The assembled LBL MWNT-COOH/PANI/ITO electrode showed high stability, low detection limit, which can be applied to the determination of NIF. It presents a good example that the electronic communications between the active substances may endow the electrode good facility, selectivity, and sensitivity to the determination of biomaterials.

ACKNOWLEDGMENTS

This work was financially supported by the National Natural Science Foundation of China (Grant No. 21103133); the Scientific Research Foundation for the Returned Overseas Chinese Scholars, State Education Ministry; the Natural Science Foundation of Shaanxi Province (No. 2015JM5224).

REFERENCES

1. Chung, D.-J.; Whittaker, A. K.; Choi, S.-H. *J. Appl. Polym. Sci.* **2012**, *126*, E28.
2. Singh, K.; Singh, B. P.; Chauhan, R.; Basu, T. *J. Appl. Polym. Sci.* **2012**, *125*, E235.
3. Kim, K.; Kim, B.-J.; Kim, K.-C.; Choi, S.-H. *J. Appl. Polym. Sci.* **2013**, *128*, 2230.
4. Pan, Y.; Zhang, Y.-Z.; Li, Y. *J. Appl. Polym. Sci.* **2013**, *128*, 647.
5. Li, D.; Huang, J.; Kaner, R. B. *Acc. Chem. Res.* **2009**, *42*, 135.
6. Palaniappan, S.; Saravanan, C. *J. Appl. Polym. Sci.* **2010**, *118*, 518.
7. Varma, S. J.; Jayalekshmi, S. *J. Appl. Polym. Sci.* **2010**, *117*, 138.
8. Dhand, C.; Das, M.; Datta, M.; Malhotra, B. D. *Biosens. Bioelectron.* **2011**, *26*, 2811.
9. Andreyev, E. A.; Komkova, M. A.; Nikitina, V. N.; Zaryanov, N. V.; Voronin, O. G.; Karyakina, E. E.; Yatsimirsky, A. K.; Karyakin, A. A. *Anal. Chem.* **2014**, *86*, 11690.
10. Ali, S. R.; Ma, Y.; Parajuli, R. R.; Balogun, Y.; Lai, W. Y.-C.; He, H. *Anal. Chem.* **2007**, *79*, 2583.
11. Meng, C.; Liu, C.; Fan, S. *Electrochem. Commun.* **2009**, *11*, 186.
12. King, R. C. Y.; Roussel, F.; Brun, J.-F.; Gors, C. *Synth. Met.* **2012**, *162*, 1348.
13. Yang, C.; Wang, X.; Du, P.; Liu, P. *Synth. Met.* **2013**, *179*, 34.
14. Wang, Q.; Qian, X.; Wang, S.; Zhou, W.; Guo, H.; Wu, X.; Li, J.; Wang, X. *Synth. Met.* **2015**, *199*, 1.
15. Feng, W.; Bai, X. D.; Lian, Y. Q.; Liang, J.; Wang, X. G.; Yoshino, K. *Carbon* **2003**, *41*, 1551.
16. Jiménez, P.; Castell, P.; Sainz, R.; Ansón, A.; Martínez, M. T.; Benito, A. M.; Maser, W. K. *J. Phys. Chem. B* **2010**, *114*, 1579.
17. Salvatierra, R. V.; Oliveira, M. M.; Zarbin, A. J. G. *Chem. Mater.* **2010**, *22*, 5222.
18. Oueiny, C.; Berlioz, S.; Perrin, F.-X. *Prog. Polym. Sci.* **2014**, *39*, 707.
19. Liu, J.; Tian, S.; Knoll, W. *Langmuir* **2005**, *21*, 5596.
20. Hu, Z.; Xu, J.; Tian, Y.; Peng, R.; Xian, Y.; Ran, Q.; Jin, L. *Carbon* **2010**, *48*, 3729.
21. Hyder, M. N.; Lee, S. W.; Cebeci, F.; Schmidt, D. J.; Shao-Horn, Y.; Hammond, P. T. *ACS Nano* **2011**, *5*, 8552.

22. Hyder, M. N.; Kavian, R.; Sultana, Z.; Saetia, K.; Chen, P.-Y.; Lee, S. W.; Shao-Horn, Y.; Hammond, P. T. *Chem. Mater.* **2014**, *26*, 5310.
23. Cheung, J. H.; Stockton, W. B.; Rubner, M. F. *Macromolecules* **1997**, *30*, 2712.
24. de Barrosa, A.; Ferreira, M.; Constantinoc, C. J. L.; Ferreira, M. *Synth. Met.* **2014**, *197*, 119.
25. Lee, S. W.; Kim, B.-S.; Chen, S.; Shao-Horn, Y.; Hammond, P. T. *J. Am. Chem. Soc.* **2009**, *131*, 671.
26. Wu, T.-M.; Lin, Y.-W. *Polymer* **2006**, *47*, 3576.
27. Sarker, A. K.; Hong, J.-D. *Colloid Surf. A: Physicochem. Eng. Aspects* **2013**, *436*, 967.
28. Diez-Caballero, R. J. B.; de la Torre, L. L.; Valentin, J. F. A.; Garcia, A. A. *Talanta* **1989**, *36*, 501.
29. Ghoneim, M. M.; Tawfik, A.; Khashaba, P. Y. *Anal. Bioanal. Chem.* **2003**, *375*, 369.
30. Baghayeri, M.; Namadchian, M.; Karimi-Maleh, H.; Beitollahi, H. *J. Electroanal. Chem.* **2013**, *697*, 53.
31. Sentürk, Z.; Özkan, S. A.; Özkan, Y. *J. Pharm. Biomed. Anal.* **1998**, *16*, 801.
32. Gaichore, R. R.; Srivastava, A. K. *Sensor. Actuat. B: Chem.* **2013**, *188*, 1328.
33. Chiang, J.-C.; MacDiarmid, A. G. *Synth. Met.* **1986**, *13*, 193.
34. Ram, M. K.; Salerno, M.; Adami, M.; Faraci, P.; Nicolini, C. *Langmuir* **1999**, *15*, 1252.
35. Wang, Q.; Zhou, W.; Wang, S.; Li, J.; Zhang, W.; Wang, X. *J. Appl. Polym. Sci.* **2014**, *131*, 40259. Doi: 10.1002/app.40259.
36. Stejskal, J.; Riede, A.; Hlavatá, D.; Prokeš, J.; Helmstedt, M.; Holler, P. *Synth. Met.* **1998**, *96*, 55.
37. Ramana, G. V.; Srikanth, V. V. S. S.; Padya, B.; Jain, P. K. *Eur. Polym. J.* **2014**, *57*, 137.
38. Wang, X.; Gao, K.; Shao, Z.; Peng, X.; Wu, X.; Wang, F. *J. Power Sources* **2014**, *249*, 148.
39. Wang, S.; Guo, H.; Wang, X.; Wang, Q.; Li, J.; Wang, X. *Langmuir* **2014**, *30*, 12923.
40. Dhand, C.; Arya, S. K.; Singh, S. P.; Singh, B. P.; Datta, M.; Malhotra, B. D. *Carbon* **2008**, *46*, 1727.
41. Zeng, G.; Gao, J.; Chen, S.; Chen, H.; Wang, Z.; Zhang, X. *Langmuir* **2007**, *23*, 11631.